Dyes and Pigments 243 (2025) 113088

Contents lists available at ScienceDirect

Dyes and Pigments

journal homepage: www.elsevier.com/locate/dyepig

A dual-responsive Dansyl–Naphthalimide system for Hg(II) CHEF detection and ligand-mediated Cu(II) reduction with catalytic relevance

Frederico Duarte [a], Diogo Torres [a], Georgi M. Dobrikov [b,c,*], Atanas Kurutos [b,d,**], Luisa B. Maia [e], Oleksandr Bondarchuk [f], Ivaylo Slavchev [b], Jose Luis Capelo-Martínez [a,g], Hugo M. Santos [a,g], Carlos Lodeiro [a,g,***]

[a] BIOSCOPE Research Group, LAQV-REQUIMTE, Chemistry Department, NOVA School of Science and Technology, FCT NOVA, Universidade NOVA de Lisboa, 2829-516, Caparica, Portugal
[b] Institute of Organic Chemistry with Centre of Phytochemistry, Bulgarian Academy of Sciences, Acad. G. Bonchev Str., Bl. 9, 1113, Sofia, Bulgaria
[c] National Centre of Excellence Mechatronics and Clean Technologies, Sofia, Bulgaria
[d] University of Chemical Technology and Metallurgy, 8 St. Kliment Ohridski Blvd, 1756, Sofia, Bulgaria
[e] LAQV-REQUIMTE, Chemistry Department, NOVA School of Science and Technology, FCT NOVA, Universidade NOVA de Lisboa, 2829-516, Caparica, Portugal
[f] International Iberian Nanotechnology Laboratory - INL, Avenida Mestre José Veiga S/n, 4715-330, Braga, Portugal
[g] PROTEOMASS Scientific Society, 2825-466, Caparica, Portugal

ARTICLE INFO

Keywords:
Dansyl
Naphtilimide
Copper(II)
Mercury(II)
Sensing
Ligand-mediated reduction

ABSTRACT

We report a compelling structure–property relationship in a series of four naphthalimide-derived ligands, engineered for the selective and differential detection of Hg(II) and Cu(II) ions. By integrating a dansyl moiety, we induce intramolecular electron transfer that gives rise to two non-redox-innocent dyad systems. Notably, the detection of Hg(II) operates through a rare chelation-enhanced fluorescence (CHEF) mechanism, an unusual pathway considering the heavy atom effect typically associated with mercury. In contrast, the Cu(II) dyads reveal striking reduction of Cu(II) to Cu(I) in solution, driven by ligand-to-metal electron transfer, as conclusively demonstrated via EPR and XPS analysis. Furthermore, introducing a catalytic substrate probe highlights that this redox transformation is the bottleneck in catalytic efficiency. These findings provide deep mechanistic insights and position these ligands as versatile platforms for dual-mode ion sensing and redox-responsive catalysis.

1. Introduction

The design of luminescent probes for heavy and transition metal ions detection have gathered substantial attention due to their impact in environmental and biological assays [1]. Among these metal ions, divalent copper is known for being the third most abundant metal ion in the human body which are crucial in a wide range of biological processes and is linked to neurodegenerative illnesses [2–4]. In turn, high toxicity is the main reason why there is a constant demand for the monitorization of mercury in the environment in order to remediate the potential threat to public health [1,5–7].

In light of the considerable progresses over the decades, dansyl and naphthalimide derivatives have been consistent fluorophores exhibiting strong biocompatibility and reliable photophysical properties. High fluorescence quantum yields, large Stokes shift and solvatochromic behavior are common characteristics related to dansyl derivatives while the tunable emission profiles of naphthalimide dyes by simple modification of the core offer the novelty and versatility as sensors towards heavy and transition metal ions [1,8,9]. Notably, the use of these dyes towards Cu(II) [10–25] and Hg(II) [6,7,26–33] are well entrenched in the literature. However, the main strategies employed for these systems often rely only on fluorescence changes in single-emission windows that

* Corresponding author. Institute of Organic Chemistry with Centre of Phytochemistry, Bulgarian Academy of Sciences, Acad. G. Bonchev Str., Bl. 9, 1113 Sofia, Bulgaria
** Corresponding author. Institute of Organic Chemistry with Centre of Phytochemistry, Bulgarian Academy of Sciences, Acad. G. Bonchev Str., Bl. 9, 1113 Sofia, Bulgaria
*** Corresponding author. BIOSCOPE Research Group, LAQV-REQUIMTE, Chemistry Department, NOVA School of Science and Technology, FCT NOVA, Universidade NOVA de Lisboa, 2829-516 Caparica, Portugal.
E-mail addresses: Georgi.Dobrikov@orgchm.bas.bg (G.M. Dobrikov), atanas.kurutos@orgchm.bas.org (A. Kurutos), cle@fct.unl.pt (C. Lodeiro).

https://doi.org/10.1016/j.dyepig.2025.113088
Received 21 June 2025; Received in revised form 30 July 2025; Accepted 30 July 2025
Available online 5 August 2025

may be hindered by environmental effects. Consequently, an increase in demand for the design of more efficient sensors that provide signal fidelity, dual-channel or ratiometric approaches have become more frequent to provide high signal-to-noise ratio and mitigate environmental interference [1,8]. Dual fluorescence probes emerge as optimal choices providing a broader window of emission with enhanced fluorescence signal modalities. Some examples explore the utility of both dansyl and naphthalimide fluorophores as excited dye donors towards Föster resonance energy transfer (FRET) systems for metal ion sensing in conjunction with rhodamines [1,5,34–38] as well as other dyes across diverse applications [8,39–42].

When considering the most desirable fluorescent sensor for metal ions, one may consider those that display chelation-enhanced fluorescence (CHEF) the best suited. However, the large spin-orbit coupling constant of Hg(II) and the paramagnetic nature of Cu(II) causes the majority of sensors towards these metals to be "turn-off" in nature [43]. Some of the aforementioned dyad systems avoid these hindrances due to the initial presence of a photoinduced electron-transfer (PeT) effect [1,5,35] that prevents an excited electron to relax radiatively to ground state since an electron from a lone pair that is higher in energy drops to the SOMO-H of the fluorophore. The coordination of the metal ion can stabilize the donor orbital lowering its energy below from the ground state restoring fluorescence with a few examples of this behavior applied in dansyl systems for the detection of Hg(II) [43–45]. Furthermore, strategic multiple-ion-responsive sensors with built-in selective and differential detection are of upmost importance with several examples reported in the literature towards Cu(II) and Hg(II) [46–48].

Among the transition-metal compounds, in some cases, it is possible to observe reversible intramolecular electron-transfer between the metal and the ligand provided that the two electronic states are close-lying, energetically speaking. Valence tautomerism or redox isomerism rises from this notion when one or more non-redox-innocent ligand coordinates with a redox-active metal center and are capable of reversibly shift the electronic charge distribution [49,50]. However, electron delocalization must be avoided so that the two valence tautomers can be differentiated. Such processes of charge-distribution expand the scope and applicability since these systems are provided with unique physical properties and are found in nature in enzymatic processes [51]. The most known valence tautomeric systems are found for cobalt using dioxolane ligands accompanied with fewer examples of other metal complexes such as manganese, nickel, iron, ruthenium and others [50,52–54]. Copper can also form valence tautomerism since electronic and structural changes between Cu(I) and Cu(II) can create a barrier in energy sufficient enough to prevent charge delocalization so that they can be distinguishable. However, examples that fall outside of dioxolane and related structures are considered as rather rare [49,51,55]. Furthermore, copper shows some advantages over other metals in terms of catalysis since it is more cost-effective and has garnered industrial interest. For this reason, copper-catalyzed cross coupling Ullmann type reactions have become a very useful process to build several types of bonds while ancillary chelating ligands have brought reliability and mildness to these systems [56–58].

In this work, four new naphthalimide derived compounds (Scheme 2, **L1** to **L4**), from which two are dansyl-substituted dyad systems were successfully synthesized. Exploration of the interaction between dansyl and naphthalimide in dyad systems, to the best of our knowledge, is not well explored with only a handful works reported [59–62]. Bearing this in mind, efforts have been put forth to establish a structure/photophysical properties relation by intentional modification of the naphthalimide core and the presence or absence of the dansyl moiety. The complete characterization of the photophysical properties in a diverse array of solvents provided the foundation for the use of the Kamlet-Taft equation to assess the solvatochromism behavior of these systems. Due to the existence of well-defined coordination sites, these fluorophores have been tested for differential detection of metal ions owing to the occurrence of energy transfer processes in dual fluorescence probes. The determination of association constants and sensing limit parameters along with metal ion selectivity experiments were implemented. ESI-HRMS was employed to follow the complex formation in solution and to compare with the synthesized isolated complexes. Moreover, electron paramagnetic resonance spectroscopy (EPR) and X-ray Photoelectron Spectroscopy (XPS) were deemed beneficial for the elucidation of the ligand-mediated chemical reduction between the dyad systems and Cu^{2+} ions. Finally, the integration of iodophenyl moiety was found fruitful to establish the usefulness of these dyad compounds as ancillary chelating ligands for copper-catalyzed reactions.

2. Results and discussion

2.1. Synthesis

For the preparation of the target compounds (**L1**-**L4**), intermediates **3**, **5**, **7**, **9**, **10** and **13** were synthesized as shown in Scheme 1. Compound of **3** (83 %) was synthesized starting from **1** and **2** in dry DMF according to a protocol reported in the literature [63–65]. The synthesis of compound **5** was described by Benati et al. [66] and Chinapang et al. [67], however our attempt furnished **5** in increased yield (82 % after crystallization). Naphthalimide **7** (89 % after crystallization) is a new compound, though an analogue is described elsewhere [68]. Synthesis of bromide **9** from **1** and amine **8** was described in multiple studies, nevertheless we followed the procedure of Lim et al. [69] as the most suitable for our investigation (almost quantitative yield of **9**). Since **9** is well characterized, we performed only ^{1}H NMR spectra to confirm its chemical structure. Like compound **7**, intermediate **10** (89 % after column chromatography) was prepared from **9** and the diamine **6** in dry *N*-methylpyrrolidone. As a new compound, it was fully characterized by various 1D and 2D NMR techniques (Figures SX 1-129, Supplementary Material), melting point temperatures, and mass spectra. Although existing literature synthetic procedures report low yielded [70–72], amine **13** was readily prepared by heating of methyl salicylate (**11**) with ethylenediamine (**12**) under solvent free conditions. Compound **13** was purified by column chromatography and isolated in good yield (66 %).

The target compounds **L1** and **L2** were prepared by heating the intermediate **7** in dry pyridine with sulfonyl chlorides **14** and **15**, respectively (Scheme 2). **L1** (54 %) and **L2** (77 %) were isolated after silica gel column chromatography. Ligand **L3** was prepared from **10** and dansyl chloride (**14**) by using the same procedure, as in case of **L1** and **L2**. However, the yield of compound **L3** (23 %) was significantly decreased, due to the need of implementation of triple column chromatography. The synthetic approach to the preparation of **L4** (14 %) involves the use of intermediates **3** and **13**. The reaction was performed in dry 2-methoxyethanol at 110 °C (Scheme 2). The target compounds **L1**-**L4** as well as all new intermediate products were fully characterized by 1D and 2D NMR spectroscopic techniques (Figs. S1–129, Supplementary Material), HRMS and melting point temperatures.

2.2. Photophysical characterization

The conjugated dansyl-naphthalimide and single naphthalimide derived compounds manifest luminescent properties both in solution and in the solid state. Fig. 1 compiles the molecular structure accompanied by the photoluminescent data of all compounds in acetonitrile recorded at 298 K as a representative example (Figure S5-S8) while Table 1 exhibits all the photophysical data of the compounds under investigation. The UV–Vis spectra in acetonitrile shows an absorption band maximum centered at 425 and 429 nm, contributing to the display of yellow solutions to the naked eye. Upon excitation at the appropriate wavelength, the samples emit a greenish yellow light with a maximum allocated around 515 nm resulting in a Stokes shift between 4150 and 3854 cm^{-1}. On a relatable note, significant disparities can be noted regarding the solid-state emission spectra since compounds **L1** to **L3**

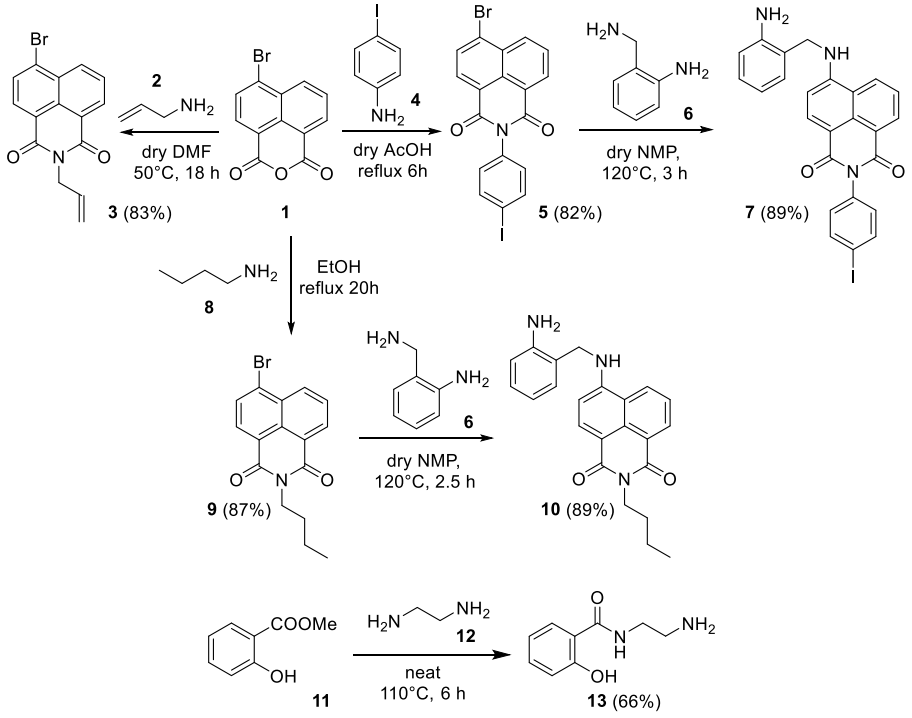

Scheme 1. Synthesis of intermediates **3**, **5**, **7**, **9**, **10** and **13**.

progressively display a red-shifted wide band centered at 528, 535 and 546 nm as in solution is concerned, while the opposite is found for **L4**, a clear, blue-shifted emission is observed with an emission maximum of 476 nm.

Overall, from a quantum yield perspective, higher values were obtained in the case of **L2** and **L4**, reaching values up to 69 % in THF, while for **L1** and **L3** the presence of the dansyl unit translates a lower general trend of values, being the fluorescent mechanism most efficient in chloroform. Single digit nanosecond times were obtained from lifetime measurements for the majority of solvents being **L1** and **L3** the ones that present more variability as each solvent is considered while more prevalent values were found for **L2** and **L4**.

Considering the well-documented solvatochromic behavior of dansyl and naphthalimide derivatives and given the visually detected solvent dependent color change under UV lamp (Fig. 1f and g), compounds **L1** to **L4** manifest positive solvatochromism due to the change in color from green to yellow with increasing solvent polarity. In line with these observations, efforts have been made to fully characterize the occurring solvent-compound interactions, and for this, three solute-dependent parameters (υ_0, a, b and p) have been determined through the multiparametric fitting of the Kamlet-Taft equation (Equation (1)).

$$\upsilon = \upsilon_0 + a\alpha + b\beta + p\pi^* \qquad \text{(Equation 1)}$$

Where υ_0 represents the wavenumber value in a reference solvent; parameters a, b and p are obtained through multiple regression analysis that reflect the underlying sensitivity of the probes photophysical behavior to solvent polarity; α: hydrogen bond donor acidity (HBD); β: hydrogen bond acceptor basicity (HBA); π*: stabilization of a charge or dipole without a specific dielectric interaction (Table S1) [73,74].

Table 2 summarizes the reference wavenumber value υ_0, the fitted parameters (a, b and p) alongside the slopes and correlation coefficients obtained through the fitting of a linear plot of $\upsilon_{exp.}$ versus υ_{calc}, by applying the Kamler-Taft model excluding acetonitrile.

Interestingly, all compounds present negative values of both a and b parameters, however, key inferences can be considered by comparing the dual and single chromophoric compounds. While the hydrogen bond donor sensitivity is roughly the same for **L1**, **L3** and **L4**, compound **L2** is 2-fold more susceptible to being influenced by protic solvents due to the quinoline group. Differences also rise in terms of sensitivity towards hydrogen bond acceptor interactions. Compound **L1** and **L3** are two-fold and three-fold less prone to be afflicted by the basic character of the solvent in regard to **L2** and **L3**, respectively. Finally, large negative p values indicate that the excited state of all compounds can be stabilized to the same degree by highly polarizable solvents.

2.3. Metal ions sensing

Given the extensive literature on the application of dansyl and naphthalimide derivatives towards the sensing of metal ions and presence of well-defined coordination sites of the compounds in investigation, additions in acetonitrile of 1, 5 and 10 equivalents Ca^{2+}, Co^{2+}, Ni^{2+}, Cu^{+}, Cu^{2+}, Zn^{2+}, Ag^{+}, Cd^{2+}, Hg^{+}, Hg^{2+} and Pb^{2+} were performed. Fig. 2 contains the normalized intensities at 515 and 513 nm of compounds **L1** and **L4** upon addition of each metal ion while **L2** and **L3** can be seen in .Figure S10

All compounds show sensitivity towards Cu^{2+} and Hg^{2+} metal ions, however, it is noteworthy to highlight a chelation enhancement of fluorescence of **L1** and **L3** towards Hg^{2+} while the exact opposite was found in the case of compound **L2** and **L4**. It is noteworthy to highlight a shift of the emission band of **L4** to 493 nm towards the sensing of Hg^{2+} that can be seen in Figure S9 and will be discussed further ahead. In terms of Cu^{2+} a general quenching of the emission was observed across all compounds.

In line with the previous results, Fig. 3 exhibits the spectrophoto- and spectrofluorimetric titrations in response to increasing concentrations of Hg^{2+} and Cu^{2+} for **L1** and **L4**, and Figure S11 for **L2** and **L3**. Overall, consecutive additions of Hg^{2+} ions cause a relative no change of the absorbance maxima centered at 425 nm for **L1** while simultaneously a gradual increase of the emission intensity is observed maintaining its maximum at around 515 nm. This change is associated with an increase in the quantum yield from 7.5 % to 24.6 % and a fluorescence decay of 9.36 ns representing an almost 2-fold increase (Fig. 3a). A similar behavior was observed for **L3** with an increase in the quantum yield to

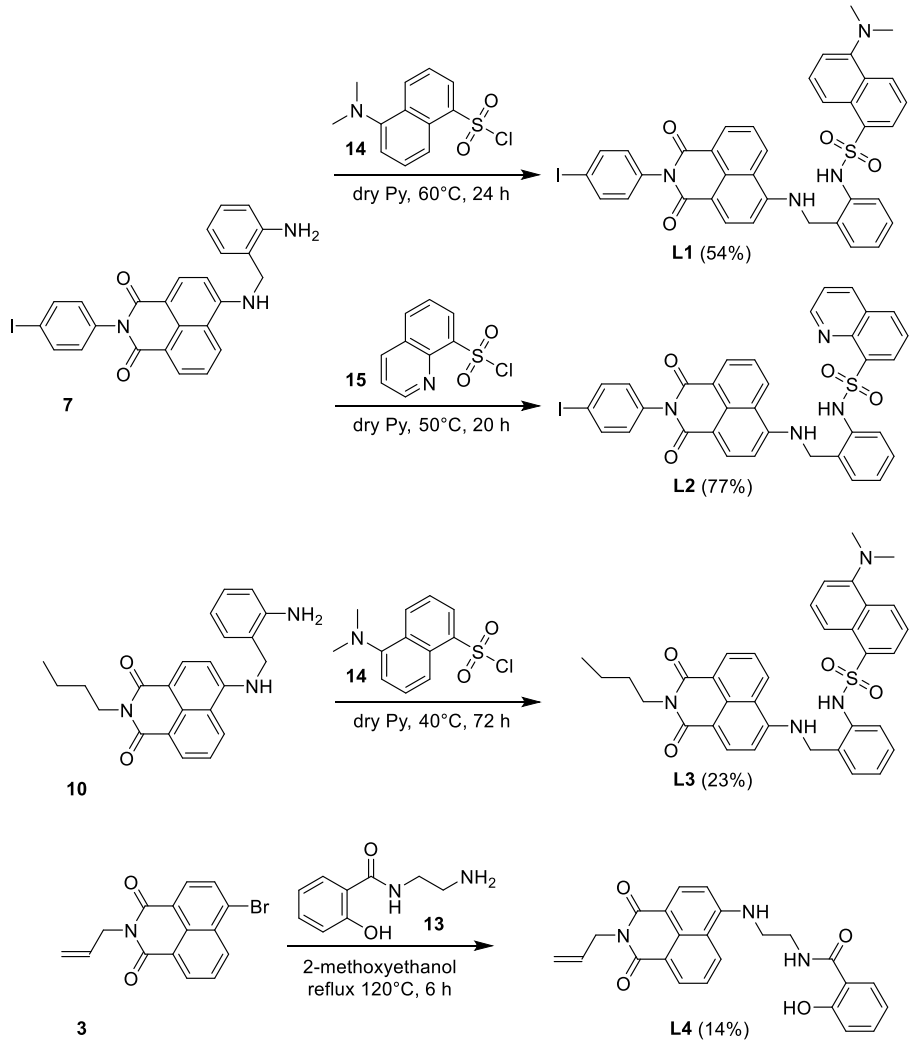

Scheme 2. Synthetic approach to the preparation of the target compounds **L1**-**L4**.

31.5 % with the same 2-fold increase in fluorescence decay to 9.31 ns (Figure S11). ESI-HRMS elucidates the formation of 2:1 (L:M) complex for **L1** (Figure S12; $[M+H]^+$ for $C_{74}H_{56}HgI_2N_8O_8S_2$ = 1705.1542 *m/z* (0.002 ppm). Calculated $[M+H]^+$ for $C_{74}H_{56}HgI_2N_8O_8S_2$ = 1705.154197 *m/z*) while a 1:1 complex has been detected for **L3** (Figure S13; $[M+H]^+$ for $C_{35}H_{32}HgN_4O_4S$ = 807.1928 *m/z* (0.05 ppm). Calculated $[M+H]^+$ for $C_{35}H_{32}HgN_4O_4S$ = 807.192756 *m/z*)

The absorption response of **L1** and **L3** during the batch titration recorded 24 h after the addition increments of 0.5 eq. of Cu^{2+} until 7 eq. and 8 eq., respectively, showed the continuous decrease of the 425 nm band leading to the emergence of a band centered at 500 nm while a quenching of the emission was observed (Figure S14). When viewed by the unaided eye a progressive transition from yellow to pink solution was evident. To better characterize this behavior the progression of the absorption profile through time was recorded and is expressed in Fig. 3b and Figure S11 for **L1** and **L3**, respectively. The results suggest the same general trend observed for the batch titration with a bathochromic shift of the absorption profile, which stabilizes around 220 min past the addition. Taking into consideration the time lapse, the formation of a complex with an inferior molecular weight than the original ligand has been found for **L1** (Figure S15; ESI-HRMS $[M+H]^+$ for $C_{39}H_{31}CuN_5O_5S$ = 745.1415 *m/z* (0.05 ppm). Calculated $[M+H]^+$ for $C_{39}H_{31}CuN_5O_5S$ = 745.141464 *m/z*) whereas for **L3,** the complex found shows no signs of ligand's cleavage at the same timepoint (Figure S16; ESI-HRMS $[M+Na]^+$ for $C_{35}H_{32}CuN_4O_4S$ = 690.1332 *m/z* (−0.07 ppm). Calculated $[M+Na]^+$ for $C_{35}H_{32}CuN_4O_4S$ = 690.133245 *m/z*) Although a better understanding of this phenomenon will be discussed and supported further ahead, early indications suggest that the iodophenyl moiety suffers changes in result of the complexation with Cu^{2+}. However, this has not demonstrated to be the limiting factor on the colorimetric response since in the absence of the iodophenyl moiety, **L3** showed the same behavior.

The introduction of the quinoline moiety in place of the dansyl unit in compound **L2** gives a stark contrast in the sensing mechanism of the aforementioned metal ions (Figure S11). In the case of Hg^{2+}, a generic quenching of the emission is observed with very few changes to the absorption profile. For Cu^{2+} an attenuation of the 427 nm absorption band and the formation of a band at around 370 nm in parallel with the quenching of the emission is observed. In this case, no changes in the resulting transparent solution of **L2** were detected in the upcoming hours after the experiment took place, highlighting the necessity for the presence of the dansyl moiety in both the turn-on effect and the colorimetric response. Complexation in 1:1 ratio has been found towards Hg^{2+} (Figure S17; ESI-HRMS $[M+H]^+$ for $C_{34}H_{21}HgIN_4O_4S$ = 911.0111 *m/z* (−0.03 ppm). Calculated $[M+H]^+$ $C_{34}H_{21}HgIN_4O_4S$ = 911.011127 *m/z*) and Cu^{2+} (Figure S18; ESI-HRMS $[M+H]^+$ for $C_{34}H_{21}CuIN_4O_4S$ = 771.9690 *m/z* (−0.9 ppm). Calculated $[M+H]^+$ $C_{34}H_{21}CuIN_4O_4S$ = 771.969698 *m/z*). Some attention should be given to the fact that, in contrast to the case of **L1**, the iodophenyl moiety of **L2** maintained its integrity demonstrating a close association between the distinct

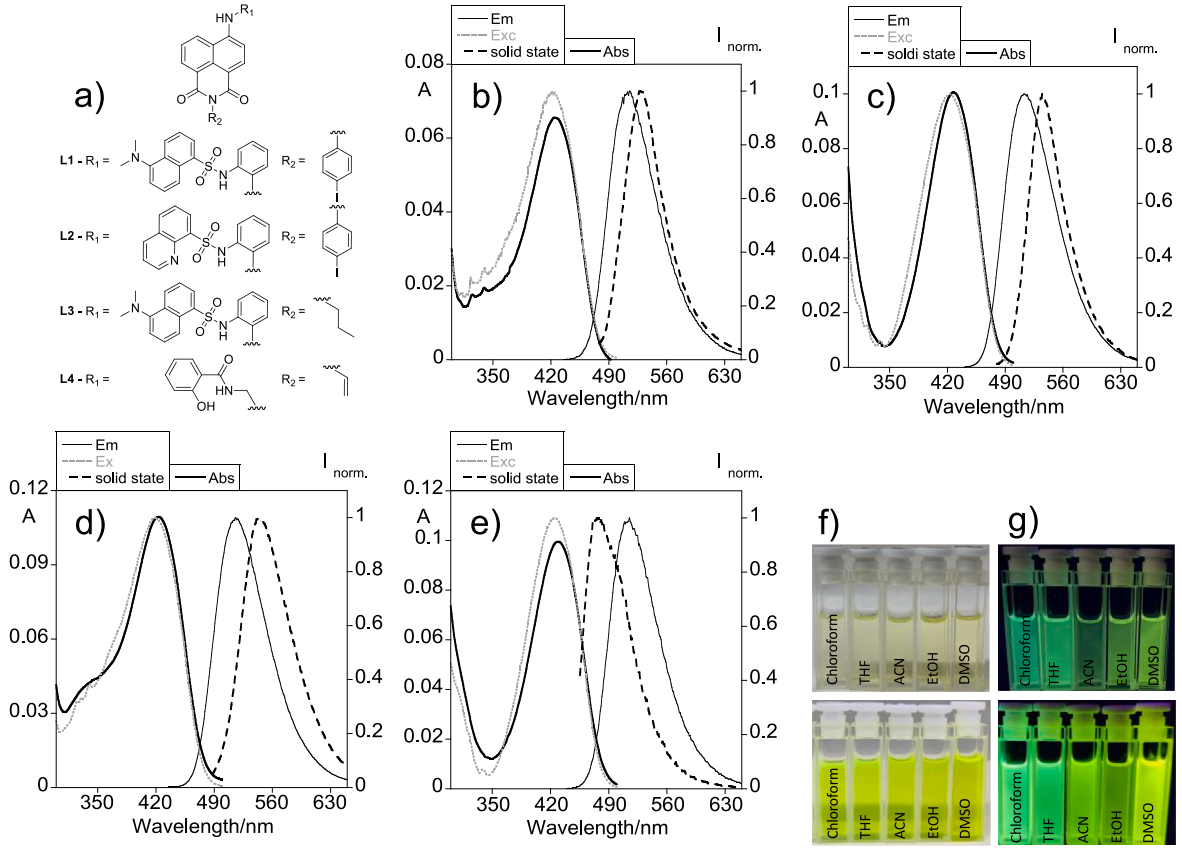

Fig. 1. (A) Molecular structure of dual dansyl-naphthalimide and naphthalimide derived compounds **L1** to **L4**. Photophysical characterization of compounds **L1** to **L4** ((b) to (e)) in acetonitrile ([**L1**] to [**L4**] = 5 μM). Images under natural light (left) and irradiated under UV light (right) for (f) **L1** and (g) **L4** in different solvents, as representative example.

Table 1
Absorption maximum wavelength in solution (λ_{abs}), emission maximum wavelength in solution (λ_{em}), molar absorption coefficients (ε), Stokes shift ($\Delta\lambda$), fluorescence quantum yields (ϕ), emission maximum in the solid state (λ_{em}^{Solid}), fluorescence lifetimes (τ) for compounds **L1** to **L4** in various solvents.

Cpd.	Solv.	λ_{abs} [nm]	λ_{em} [nm]	ε (10^4) [cm^{-1} M^{-1}]	Stokes shift [cm^{-1}]	ϕ (%)	λ_{em}^{Solid} [nm]	τ[ns]
L1	DMSO	437	520	2.18	3652	15	528	5.9
	EtOH	439	521	1.99	3585	18		6.7
	CH_3CN	425	515	2.15	4111	7.5		3.3
	THF	425	497	1.70	3408	24		5.3
	$CHCl_3$	422	502	2.04	3776	33		7.1
L2	DMSO	438	521	2.09	3637	46	535	8.5
	CH_3CN	427	513	1.92	3926	35		7.5
	THF	427	498	1.74	3338	39		6.7
	$CHCl_3$	430	505	1.61	3453	53		8.0
L3	DMSO	448	516	2.17	2942	4.3		5.9
	EtOH	438	518	2.23	3526	20		7.1
	CH_3CN	425	516	2.16	4150	8.4	546	3.2
	THF	424	494	1.90	3342	26		5.6
	$CHCl_3$	418	499	1.51	3883	32		7.3
L4	DMSO	442	524	1.84	3540	43	476	10.3
	EtOH	438	523	1.61	3710	37		9.2
	CH_3CN	429	514	1.85	3854	44		10.4
	THF	426	497	1.81	3353	69		9.3
	$CHCl_3$	427	494	1.98	3176	42		9.1

properties of **L1** and Cu^{2+} ions.

Furthermore, the sensing abilities of compound **L4** towards Hg^{2+} ions are characterized by the progressive formation of a red-shifted band with a maximum centered at 465 nm accompanied by a shoulder at 445 nm. With respect to the emission spectra, a progressive quenching on its intensity is observed with the emergence of an emission maximum at 493 and a shoulder at 518 nm. Fluorescence decay curves set the initial emission with a lifetime of 10.4 ns that after addition of Hg^{2+} ions decreases to a lifetime value of 5.1 ns. The formation of a 1:1 complex towards Hg^{2+} has been detected using **L4** (Figure S19; ESI-HRMS $[M+H]^+$ for $C_{24}H_{19}HgN_3O_4$ = 616.1159 *m/z* (0.02 ppm). Calculated $[M+H]^+$ for $C_{24}H_{19}HgN_3O_4$ = 616.115890 *m/z*) The sensing capabilities of **L4** towards Cu^{2+} focus on the suppression of the absorption band and the rise of a new band centered at 350 nm while a continuous quenching

Table 2
Independent fluorescence wavenumber ($\upsilon 0$), solvent polarity (p), HBD (a), HBA (b), slope and coefficient (R^2) of the linear fitting plot $\upsilon_{exp.}$ versus $\upsilon_{calc.}$

	υ_0	a	b	p	Slope	R [2]
L1	21474	−1053	−481	−1878	1.00	1.00
L2	21500	−2134	−753	−1733	1.00	1.00
L3	21556	−1066	−468	−1821	1.00	1.00
L4	21855	−979	−1167	−1884	1.00	1.00

of the emission is observed until the addition of 10 eq. of the metal ion. For this case, ESI-HRMS suggests a 2:1 complex (Figure S20; ESI-HRMS $[M+H]^+$ for $C_{48}H_{40}CuN_6O_8$ = 892.2277 *m/z* (0.07 ppm). Calculated $[M+H]^+$ for $C_{48}H_{40}CuN_6O_8$ = 892.227636 *m/z*).

Given the results observed for the dyad systems **L1** and **L3**, we propose that these compounds manifest a photoinduced electron transfer in solution, the coordinating Hg^{2+} metal ion subsequently stabilizes the donor orbital lowering its energy further below from the ground state preventing PeT and restoring fluorescence. Hyunjung Lee et al. [43] highlighted this reasoning in modulating the fluorescence properties of Hg^{2+} complexes with also several examples reported in the literature of the turn-on sensing of Hg^{2+} [75]. In accordance with these observations and keeping in mind that PeT behavior can also be mitigated by protonation, several eq. additions of H^+ were performed for **L1** and **L3** demonstrating the same increase in fluorescence (Figure S21). Lifetime measurements help consolidate these findings with very similar increases of the decay's curves to 9.34 and 9.47 ns for **L1** and **L3**, respectively, a phenomenon much comparable as observed towards Hg^{2+} ions.

These factors facilitate the comprehension of the highly coveted potential to detect both Hg^{2+} and Cu^{2+} in the same system without falling in the predicament of the "turn-off" behavior due to the large spin-orbit coupling constant of Hg^{2+} and the paramagnetic nature of Cu^{2+}. The incorporation of the dansyl unit enables dual-function sensing: a "turn-on" fluorescence response for Hg^{2+} detection and a distinct colorimetric response for Cu^{2+} with the overall detection mechanisms depicted in Fig. 4. The colorimetric detection of Cu^{2+} will be discussed in more detail further ahead.

2.4. *Anti-interference performance in Hg^{2+} detection*

The interference effect that metal ions might promote on the turn-on detection ability of **L1** and **L3** for Hg^{2+} has been investigated by the addition of 10 eq. of each metal to a solution of each compound already containing 5 eq. of Hg^{2+}. As shown in Fig. 5 and Figure S22, the Hg^{2+} dependent fluorescence emission was not significantly altered by the presence of Ca^{2+} and the transition metal ions Co^{2+}, Ni^{2+}, Cu^{+}, Zn^{2+}, Ag^{+}, Cd^{2+}, Hg^{+}, and Pb^{2+} except for Cu^{2+} that causes a decrease in the enhanced fluorescent response towards Hg^{2+}. This behavior could be attributed to the paramagnetic nature of Cu^{2+} that may interact to different sites in the molecule or accept electrons from fluorophore's excited state. Furthermore, compound **L3** was found susceptible to water molecules in which Hg^{+} and Pb^{2+} were dissolved, exhibiting interference on the interpretation of these metal ions.

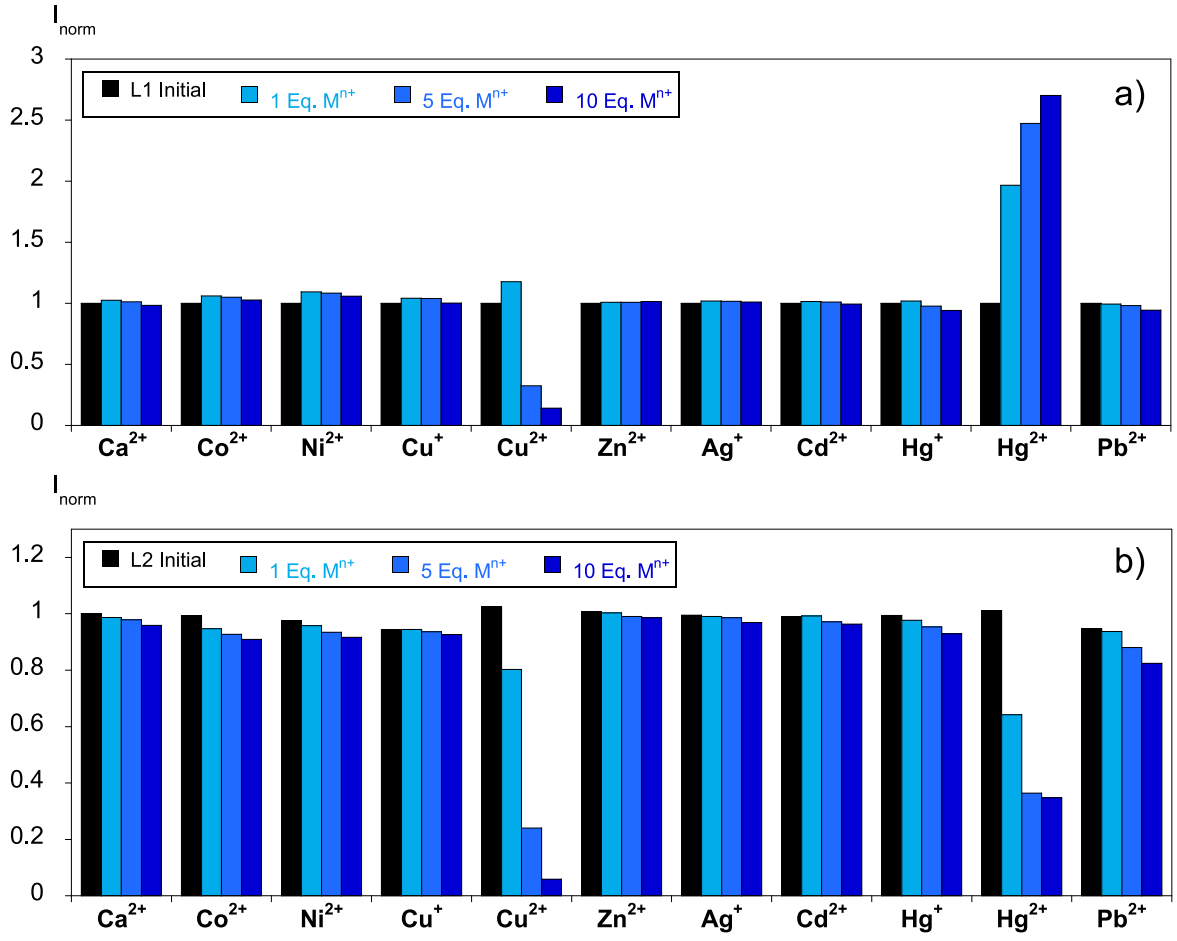

Fig. 2. Normalized emission intensity of **L1** (a) and **L4** (b) upon addition of 1, 5, and 10 equivalents of Ca^{2+}, Co^{2+}, Ni^{2+}, Cu^{+}, Cu^{2+}, Zn^{2+}, Ag^{+}, Cd^{2+}, Hg^{+}, Hg^{2+} and Pb^{2+} metal ions. ([**L1**] = [**L4**] = 10 μM, λ_{emL1} = 515 nm, λ_{emL4} = 513 nm, T = 298 K).

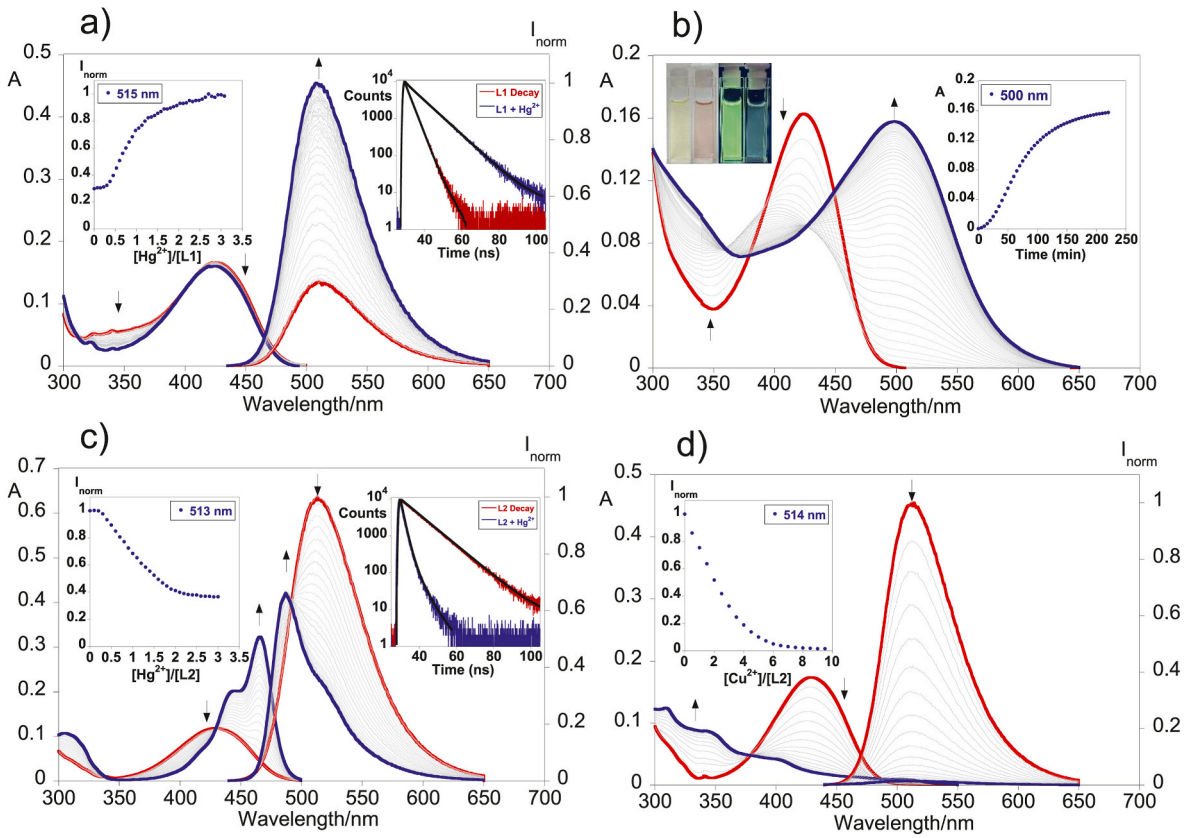

Fig. 3. UV–Vis and luminescent titration of compound **L1** (a) upon continuous 10 μL additions of Hg^{2+} ([**L1**] = 10 μM; [Hg^{2+}] = 0.225 mM). The inset represents the emission of [Hg^{2+}]/[**L1**] at 515 nm (left) and the time-resolved fluorescence decay profile of **L1** before and after the titration with Hg^{2+} ions (right). UV–vis time continuous spectra of **L1** (b) after the addition of 7 eq. of Cu^{2+} ([**L1**] = 10 μM). The inlet represents the images under natural light and UV light (left) and the time-dependent response of the absorbance at λ = 500 nm (right). UV–Vis and luminescent titration of compound **L4** (c) upon continuous 10 μL additions of Hg^{2+} ([**L4**] = 5 μM; [Hg^{2+}] 0.15 mM). The inlet represents the emission of [Hg^{2+}]/[**L4**] at 513 nm (left) and the time-resolved fluorescence decay profile of **L4** before and after the titration with Hg^{2+} ions (right). UV–Vis and luminescent titration of compound **L4** (d) upon continuous 10 μL additions of Cu^{2+} ions ([**L4**] = 10 μM; [Cu^{2+}] = 1.5 mM). The inlet represents the emission of [Cu^{2+}]/[**L4**] at 514 nm. For clarity of the reader the red spectrum represents the initial spectrum and the blue at the end point of the titration while the black curves in the fluorescent decay profile represent the fitting obtained. (For interpretation of the references to color in this figure legend, the reader is referred to the Web version of this article.)

2.5. Determination of association constants and sensing limit parameters

In order to completely assess the sensing ability of all compounds towards Hg^{2+} and Cu^{2+}, the HypSpec software [76] was used for the evaluation of the stability constants. Also, the determination of the detection and the quantification limit parameters towards both metal ions has been fulfilled. The association constants, LOD and LOQ are summarized in Table 3.

Table 3 reveals the association constants considering the stoichiometry 2:1 and 1:1 (L:M) for Hg^{2+} and Cu^{2+} in accordance with the data obtained from mass spectrometry for complex formation is concerned. The constants that relate to the stoichiometry of 2:1 were found to be very similar using **L1** and **L4** for Hg^{2+} and Cu^{2+}, respectively. Among the remaining systems, stoichiometry 1:1 was prevalent, attributing to **L2** the highest association constant towards Hg^{2+} with an association constant of 5.54 ± 0.03. In terms of LOD and LOQ, values were found to range between 1 to 8 and 2–12 μM, respectively, attributing the lowest values for the sensing of Hg^{2+} using **L3**.

2.6. Characterization of L1 and L3 complexes with Hg^{2+} and Cu^{2+}

Given the extensive studies in solution that provided the complete framework for the differentiation towards the sensing of Hg^{2+} and Cu^{2+} using **L1** and **L3**, our interest shifted in the direction of obtaining the complexes in solid form. All complexes were successfully synthesized, and a complete description of the procedures can be found in the experimental section.

The structural characterization of the complexes was achieved by FTIR and the proposed formulations were also confirmed by HRMS. The solid-state FTIR spectra of **L1** and **L3** provided the expected bands for the dansyl and naphthalimide moieties (Figures S22-S27). Complexes of **L1** showed the broadening of the 3500 to 3000 cm^{-1} regions especially the band dedicated to the ν(*N*–H) with the unchanged profile of the dicarboximide group, between 1680 and 1575 cm^{-1}, suggesting the well stablished coordination site of the secondary amines spacer. Furthermore, the dedicated region for the ν(S═O) + ν(*C*–N) bands, between 1350 and 1130 cm^{-1}, showed an increase in strength due to the presence of the triflate counterion, consolidating this finding. Concerning the Cu^{2+} complex, the increase of the bands at 2915 and 2850 cm^{-1} suggests a change in the molecular structure. The ESI-HRMS spectrum suggests the formation of a 2:1 (L:M) Hg^{2+} complex with a *m/z* of 1706.1620 (Figure S29) in accordance with the findings in solution. In turn, a smaller ion than the ligand with a *m/z* of 747.1571 (Figure S30) was found for the Cu^{2+} complex similarly detected in solution, as mentioned previously which help illustrate the emergence of the band typically associated with aliphatic *C*–H stretches found in the FTIR spectrum. Thus, this demonstrates that iodine is no longer present in the molecular structure and will be discussed further ahead.

The complexation of Hg^{2+} and Cu^{2+} with compound **L3** shares the same changes in comparison to **L1**, broadening of the 3500 to 3000 cm^{-1}

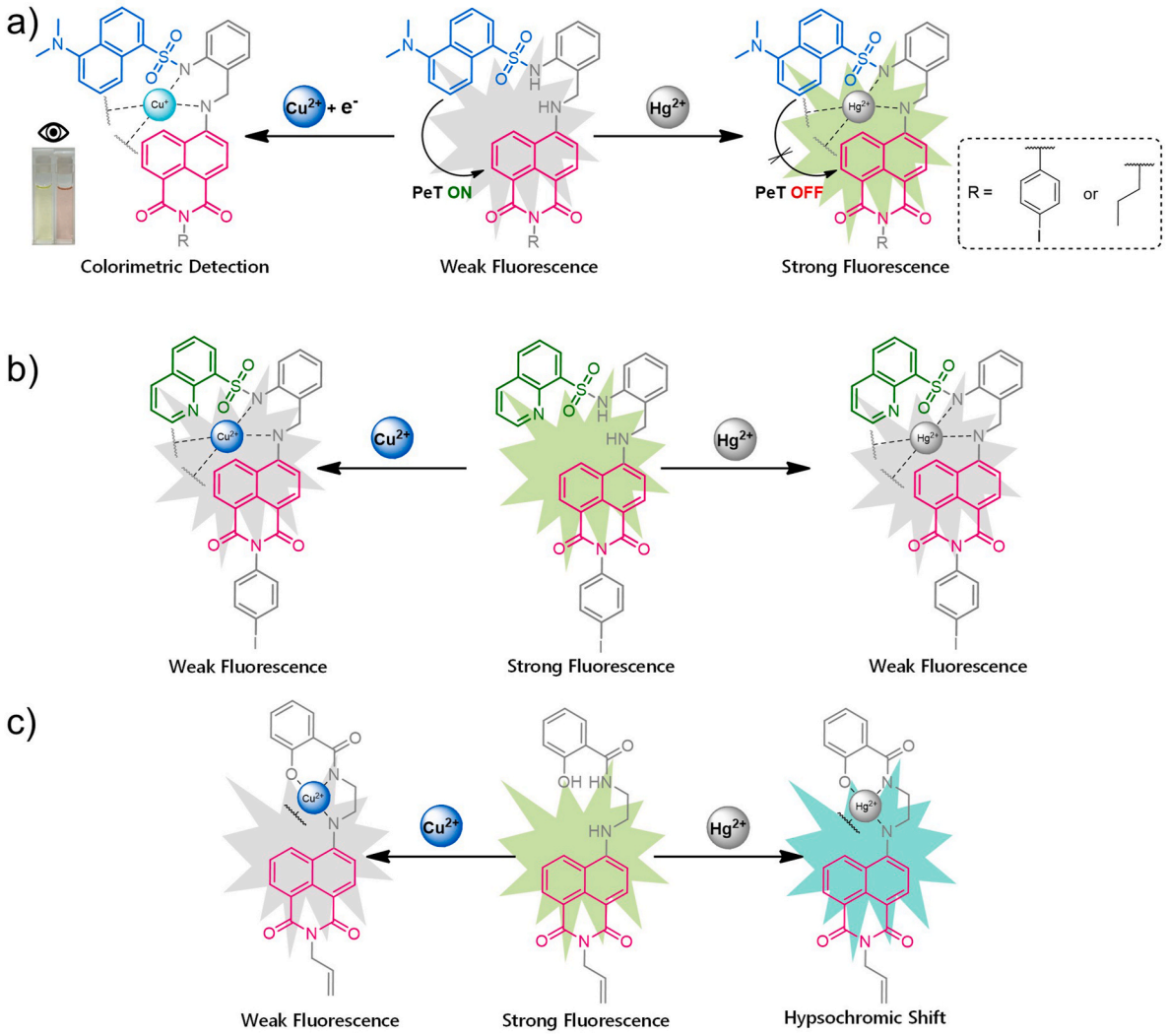

Fig. 4. Proposed mechanism after complexation with Cu^{2+} and Hg^{2+} metal ions for (a) **L1** and **L3**, (b) **L2** and (c) **L4**.

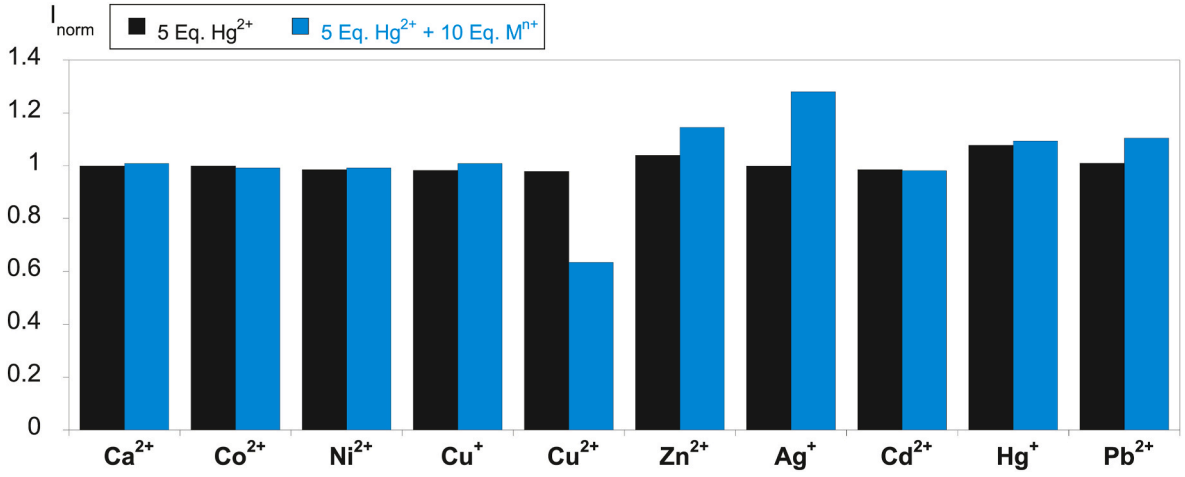

Fig. 5. Normalized emission response of **L1** in the presence of 5 equivalents Hg^{2+} and upon the addition of metal ions in acetonitrile. ([**L1**] = 10 μM, λ_{emL1} = 515 nm, T = 298 K).

region while keeping the dicarboximide profile and the increase of the ν(S═O) + ν(*C*–N) bands suggesting the presence of triflate counterion. Both complexes were followed by ESI-HRMS giving insight of the formation of a 1:1 Hg^{2+} complex with an *m/z* of 807.1929 (Figure S31) as it was found in solution, whereas the Cu^{2+} complex would preferably adopt a 2:1 stoichiometry in the solid state with an *m/z* of 1274.3814

Table 3
Association constants evaluated employing HypSpec software for compounds **L1** to **L4** towards Hg^{2+} and Cu^{2+} ions with included stoichiometry in acetonitrile. Respective values for the detection limit (LOD) and quantification limit (LOQ) amounts (μM).

Compounds	Metal (M)	Association constants ($LogK_{ass.}$), L:M	LOD (μM)	LOQ (μM)
L1	Hg^{2+}	9.39 ± 0.01 (2:1)	5.1	7.3
L2	Cu^{2+}	4.83 ± 0.03 (1:1)	8	12
	Hg^{2+}	5.54 ± 0.03 (1:1)	2.5	5
L3	Hg^{2+}	5.07 ± 0.04 (1:1)	1	2
L4	Cu^{2+}	9.37 ± 0.05 (2:1)	5	9.9
	Hg^{2+}	4.73 ± 0.04 (1:1)	3.9	7.1

(Figure S32).

2.7. Interaction mechanism study of L1 with Cu^{2+}

To shed more light on the phenomenon underlying the **L1** and **L3** photophysical characteristics upon the introduction of Cu^{2+}, the time evolution of the **L1**:Cu^{2+} complex was studied by means of EPR and X-ray photoelectron spectroscopy.

At 1:4, the EPR of L1:Cu^{2+} displays a broad axial spectrum, characteristic of Cu^{2+} (Fig. 6a, brown line), with $g// > g_{\perp} > 2$, where only two of the expected copper four $g//$ lines are visible. No super-hyperfine interactions were identified. Noteworthy, L1:Cu^{2+} displays the same key spectral features as Cu^{2+} (in acetonitrile solution, without L1; Fig. 6a, green line), indicating that only copper not coordinated to L1 is being observed in the EPR spectrum of L1:Cu^{2+}. The spectrum likely arises from heterogeneous copper species coordinated by four oxygen atoms, as suggested by the $g// \approx 2.414$ and $A// \approx 138 \times 10^{-4} cm^{-1}$ values [77].

The L1:Cu^{2+} 1:4 spectrum intensity decreases with time (Fig. 6b, light blue line), clearly showing that Cu^{2+} is being reduced to the EPR silent Cu^{+}, and, after 75 min (Fig. 6a, light orange line), almost all copper (2.0 mM) was reduced. For L1:Cu^{2+} 1:7 and 1:10, similar spectra were obtained and their intensity also decreased with time (Fig. 6b, blue and dark blue lines, respectively). These results clearly demonstrate that L1 reduces copper. Moreover, because no spectral evidence of a L1:Cu^{2+} complex was observed, these results suggest that copper is reduced upon coordination/reaction with L1 (reduction would take place within 30–60s, the minimum time required to mix L1 and copper and freeze the solution, under our experimental conditions).

To be able to reduce copper, L1 needs to be oxidized by one electron, giving rise to an initial (transient) cation radical species, $L1^{\bullet+}$. The observation of such radical is dependent on its lifetime and, if the species is present in a low accumulated concentration, its EPR signal can be greatly obscured by the broad copper signal. In this context, the small feature at $g \approx 2.004$ observed in the 45 s spectra of **L1**:Cu^{2+} 1:4 (Fig. 6a, brown line) can be taken as an evidence of a radical formation in very low amounts; for longer times, no such feature can be identified. Alternatively, **L1** can be oxidized by two electrons to yield 2 Cu^{+}. After the initial (1 or 2-electron) oxidation, each **L1** molecule ought to undergo additional oxidation events, involving a total of four electrons, to account for the complete copper reduction observed in **L1**:Cu^{2+} 1:4 after 75 min (Fig. 6a, light orange line, and Fig. 6b, light blue line). Noteworthy, when an excess of copper is used (**L1**:Cu^{2+} 1:7 and 1:10), the amount of Cu^{2+} reduced is approximately the same. For a **L1**:Cu^{2+} 1:4 (0.5:2.0 mM) ratio, (almost) no copper remains in the Cu^{2+} state; for 1:7 (0.5:3.5 mM) and 1:10 (0.5:5.0 mM) ratios, approximately 1.5 (3.5–2.0) and 3 (5.0–2.0) equivalents remain in the Cu^{2+} state, respectively (Fig. 6b). These results give further support to the suggestion that **L1** is able to promote a global 4-electron redox process with copper.

X-ray photoelectron spectroscopy was deployed to further gain insight into the oxidation states of Cu in the compounds under study after various treatments. Fig. 7a presents Cu2p spectra for the **L1**:Cu^{2+} compound with a concentration ratio of 1:4 as prepared (black curve) and after 4 h in a vacuum (red curve). Fig. 7b presents Cu2p spectra for the **L1**:Cu^{2+} compound with a concentration ratio of 1:1 as prepared (green curve) and for the $[Cu(II)\mathbf{L1}]^{2+}$ complex. All the Cu2p spectra have a complex multipeak structure, which includes doublets due to spin-orbit splitting (Cu2p3/2 and Cu2p1/2 peaks) and satellites in the binding energy range of ~938–948 eV. The complex structure of the

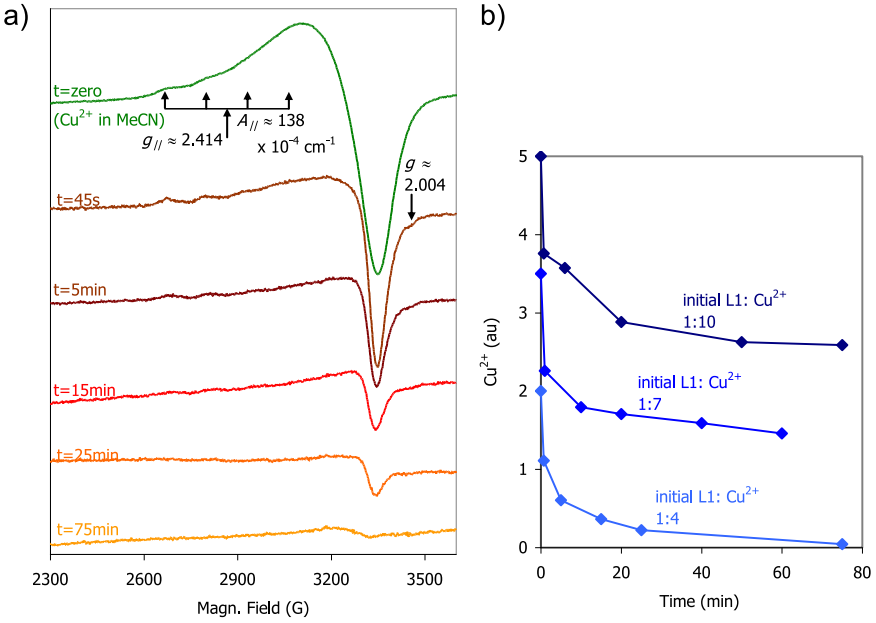

Fig. 6. (A) EPR spectra at 77 K of L1:Cu^{2+} 1:4 (0.5 mM:2.0 mM) in MeCN, at time zero (green line) and after 45s (brown), 5 min (dark red), 15 min (red), 25 min (orange) and 75 min (light orange). (b) Cu^{2+} reduction as a function of time, upon mixing L1 and Cu^{2+} at 1:4 (0.5:2.0 mM; light blue line), 1:7 (0.5:3.5 mM; blue) and 1:10 (0.5:5.0 mM; dark blue) ratios. Cu^{2+} concentration values (in arbitrary units, au) were determined from the respective EPR spectra intensity (double spectrum integration). (For interpretation of the references to color in this figure legend, the reader is referred to the Web version of this article.)

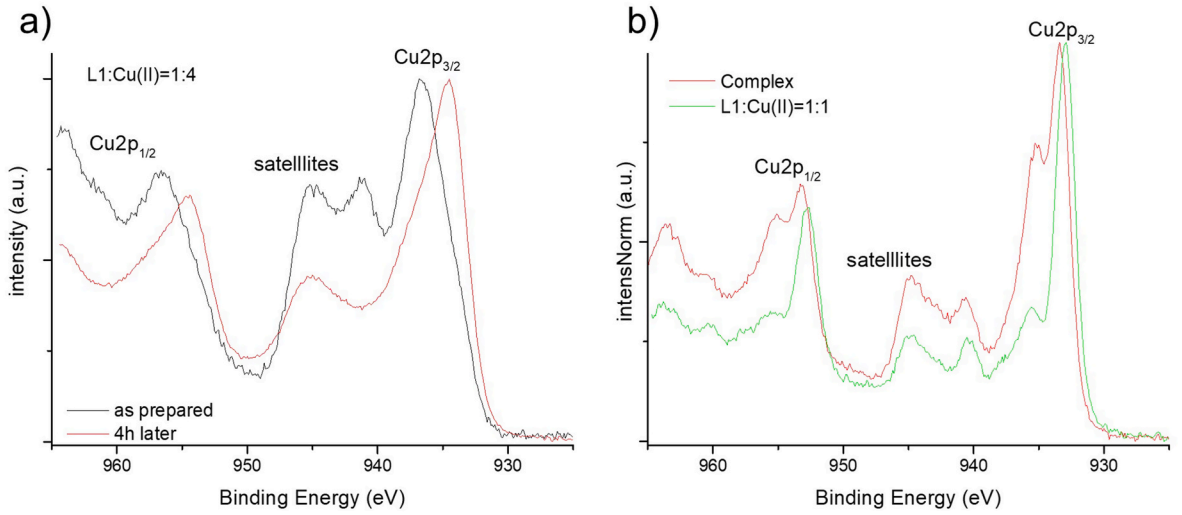

Fig. 7. Cu2p XPS spectra (a) after the addition of **L1** and Cu^{2+} in proportion 1:4 as prepared and 4 h later while (b) exhibits the spectra of the [Cu(II)**L1**]$^{2+}$ complex and in proportion 1:1 (L:M).

Cu2p XPS spectra indicates a mixture of copper oxidation states. Strong satellites in the Cu2p spectra are an indication of the Cu^{2+} oxidation state [78].

The Cu2p3/2 peaks in the spectra of the **L1**:Cu^{2+} = 1:4 compound (Fig. 7a) as prepared and after 4 h, show a wide, asymmetric shape with peak positions shifted to 933–935 eV. In the case of the **L1**:Cu^{2+} = 1:1 and [Cu(II)**L1**]$^{2+}$, the Cu2p3/2 peaks split into two components with maximum positions at ~933 and ~935 eV. Given the position of the main peak at ~933 eV and the presence of satellites, one can tentatively conclude that the **L1**:Cu^{2+} = 1:1 and [Cu(II)**L1**]$^{2+}$ compounds contain a mixture of Cu^{1+} and Cu^{2+} species. An interesting observation is the splitting of the main Cu2p3/2 peak with an additional maximum at ~935 eV. The trivial explanation for this peak would be to assign it to an oxidation state higher than 2+. However, this peak splitting appears similar to that observed in the Ni2p spectra of NiO and is often mistakenly assigned to Ni^{3+}. It has been shown that the 2p peak splitting can be explained by the nonlocal screening of the core hole created during ionization of the 2p level by electrons donated by nearest and non-nearest ligands, while maintaining the 2+ oxidation state of Ni ions [79].

It is noteworthy to analyze the relative intensity of the satellite peaks with respect to the intensity of the main Cu2p3/2 peaks. Fig. 7a, shows that the relative intensity of the satellites substantially decreased after 4 h. In the case of the **L1**:Cu^{2+} = 1:1 compound, the relative satellite intensities are smaller than those in the **L1**:Cu^{2+} = 1:4 compound. The decrease in satellites can indicate the reduction of Cu^{2+} species by mixing with the **L1** substance. After 4 h, Cu^{2+} species are still present in the **L1**:Cu^{2+} = 1:4 compound as well as in the **L1**:Cu^{2+} = 1:1 compound, as evidenced by the Cu2p XPS spectra. This could also be due to surface oxidation of the studied materials, which is detectable by the surface-sensitive XPS technique (information depth up to ~10 nm).

Provided the evidence that showed the copper reduction using **L1** and **L3** from EPR and XPS experiments and bearing in mind the PeT process that could be mitigated and applied for the sensing of Hg^{2+}, we propose that both compounds perform a ligand-mediated chemical reduction of Cu^{2+} to Cu^{+}. The presence of an intramolecular electron-transfer process leads to a shift of the electronic charge distribution and the identification of the Cu^{+} state, that can also be colorimetrically identified with a change in the absorption profile from yellow to pink. Given the absence of any indication of reversibility or equilibrium between Cu^{2+} and Cu^{+} states provided by EPR data, these systems cannot achieve valence tautomerism. Furthermore, the introduction of iodophenyl serves as a catalysis substrate probe, in which only **L1** was able to catalyze the cleavage of the carbon-iodine bond from within itself. This is mediated by the formation of the Cu^{+} complex evidenced by the formation of a complex with lower molecular weight. The reduction of copper was found the limiting factor since compound **L2**, that does not manifest intramolecular electron-transfer, would not catalyze the carbon-halogen bond given that does not reduce the copper ion. Thus, we propose that **L1** self-catalyzed an amidation of benzene through an Ullman-type reaction using acetonitrile as amino source demonstrating in this way the usefulness of these dyad systems for catalysis [56–58].

3. Conclusions

In summary, we report the synthesis and characterization of four new naphthalimide derived ligands for the differential detection of Hg (II) and Cu(II) ions. Photophysical characterization in various solvents prompted us to characterize the solvent-compound interactions through the multiparametric fitting of the Kamlet-Taft equation and underlying solvatochromism. An understanding of the photophysical properties in dyad systems has been accomplished by comparison between the introduction of a quinoline or dansyl moiety to the naphthalimide core. Intramolecular electron transfer was possible in two compounds by introduction of a dansyl moiety constituting in two non-redox-innocent dyad systems. Application of these compounds to the sensing of metal ions, particularly of Hg(II) and Cu(II) ions, proved to be effective in avoiding the well-known suppression that these ions cause to fluorescent systems. A clear turn-on or CHEF effect of the emission was detected while sensing Hg(II) ions since it lowers the energy of the lone pair further from the ground state that would cause the initial quenching. A differential detection of Cu(II) ions was achieved by a colorimetric response accompanied by the intramolecular electron transfer. In this case, the two electronic states of the non-redox-innocent ligand and the redox-active metal center are close enough to observe ligand-mediated chemical reduction of Cu^{2+}. Application of EPR and XPS provided the evidences to establish a reduction of the copper(II) center to copper(I) promoted by the underlying close connection between the dansyl and naphthalimide units of the dyad. Finally, the resulting copper complexes were found the only suited compounds to be tested in the future for their catalysis properties since the cleavage of the carbon-halogen bond implemented as a probe was only mediated by prior reduction to copper (I).

CRediT authorship contribution statement

Frederico Duarte: Writing – review & editing, Writing – original draft, Validation, Software, Methodology, Investigation, Formal analysis, Data curation. **Diogo Torres:** Writing – original draft, Visualization, Methodology, Investigation. **Georgi M. Dobrikov:** Writing – review & editing, Writing – original draft, Validation, Resources, Investigation, Funding acquisition, Formal analysis, Conceptualization. **Atanas Kurutos:** Writing – review & editing, Writing – original draft, Visualization, Supervision, Resources, Methodology, Investigation, Funding acquisition, Formal analysis, Conceptualization. **Luisa B. Maia:** Writing – review & editing, Writing – original draft, Resources, Investigation, Formal analysis. **Oleksandr Bondarchuk:** Writing – original draft, Resources, Methodology, Investigation, Formal analysis. **Ivaylo Slavchev:** Writing – original draft, Methodology, Investigation. **Jose Luis Capelo-Martínez:** Writing – review & editing, Writing – original draft, Validation, Resources, Methodology, Funding acquisition, Formal analysis, Data curation. **Hugo M. Santos:** Writing – review & editing, Writing – original draft, Visualization, Validation, Resources, Investigation, Funding acquisition, Formal analysis, Data curation. **Carlos Lodeiro:** Writing – review & editing, Writing – original draft, Visualization, Validation, Supervision, Software, Resources, Project administration, Methodology, Investigation, Funding acquisition, Formal analysis, Data curation, Conceptualization.

Declaration of competing interest

The authors declare that they have no known competing financial interests or personal relationships that could have appeared to influence the work reported in this paper.

Funding

This work received support from PT national funds (FCT/MCTES, *Fundação para a Ciência e Tecnologia* and *Ministério da Ciência, Tecnologia e Ensino Superior)* through the projects UIDB/50006/2020 and UIDP/50006/2020. This work received support from PROTEOMASS Scientific Society through the General Funding Grant 2024–2025, and the projects #PM001/2019 and #PM003/2016. This work is also developed and acknowledged by A.K. as part of contract N⍰: BG-RRP-2.004-0002-C01, Laboratory of Organic Functional Materials (Project BiOrgaMCT), Procedure BG-RRP-2.004 „Establishing of a network of research higher education institutions in Bulgaria“, funded by BULGARIAN NATIONAL RECOVERY AND RESILIENCE PLAN“.

Declaration of competing interest

The authors declare the following financial interests/personal relationships which may be considered as potential competing interests: Given his role as Executive Editor, Professor Carlos Lodeiro Y Espiño had no involvement in the peer review of this article and had no access to information regarding its peer review. Full responsibility for the editorial process for this article was delegated to another journal editor.

Acknowledgements

This work was financed by national funds from FCT - Fundação para a Ciência e a Tecnologia, I.P., under the scope of the project UID/50006/2023 of the Associate Laboratory for Green Chemistry - LAQV REQUIMTE. PROTEOMASS Scientific Society (Portugal) is acknowledged by the funding provided through the General Funding Grant 2024–2025, and by the funding provided to the Laboratory for Biological Mass Spectrometry Isabel Moura (#PM001/2019 and #PM003/2016). F.D. thanks to FCT/MCTES (Portugal) for his doctoral grant 2021.05161. BD. H. M. S. acknowledges the Associate Laboratory for Green Chemistry LAQV (LA/P/0008/2020) funded by FCT/MCTES for his research contract. This work was supported by the Associate Laboratory for Green Chemistry - LAQV (UIDB/50006/2020 (DOI: 10.54499/UIDB/50006/2020) and UIDP/50006/2020 (DOI: 10.54499/UIDP/50006/2020)), which are financed by national funds from Fundacão para a Ciência e a Tecnologia, MCTES (FCT/MCTES). LBM also thanks to FCT/MCTES, for the CEEC-Ind Program Contract. C.L. and H. M.S thanks the Royal Society of Chemistry for the Sustainable Laboratory Grants 2023 reference L23-8861107285.

The financial support by the Bulgarian National Science Fund (BNSF) under grant – “Novel styryl and polymethine fluorophores as potential theranostic agents ”contract N◦ КП-06-M59/1 from November 15, 2021 is gratefully acknowledged by A.K. This work is also developed and acknowledged by A.K. as part of contract N⍰: BG-RRP-2.004-0002-C01, Laboratory of Organic Functional Materials (Project BiOrgaMCT), Procedure BG-RRP-2.004 „Establishing of a network of research higher education institutions in Bulgaria“, funded by BULGARIAN NATIONAL RECOVERY AND RESILIENCE PLAN“.

G. D. thanks to the European Regional Development Fund within the Operational Programme Science and Education for Smart Growth 2014–2020 under the Project Center of Excellence: National center of mechatronics and clean technologies - BG05M2OP001-1.001-0008 for the financial support.

Appendix A. Supplementary data

Supplementary data to this article can be found online at https://doi.org/10.1016/j.dyepig.2025.113088.

Data availability

Data will be made available on request.

References

[1] Yuan X, Leng TH, Guo ZQ, Wang CY, Li JZ, Yang WW, Zhu WH. A FRET-Based dual-channel turn-on fluorescence probe for the detection of Hg^{2+} in living cells. Dyes Pigments 2019;161:403–10. https://doi.org/10.1016/j.dyepig.2018.09.078.

[2] Wang Y, Zhou J, Zhao L, Xu B. A dual-responsive and highly sensitive fluorescent probe for Cu^{2+} and pH based on a dansyl derivative. Dyes Pigments 2020;180:108513. https://doi.org/10.1016/j.dyepig.2020.108513.

[3] Wei P, Xiao L, Gou Y, He F, Zhou D, Liu Y, Xu B, Wang P, Zhou Y. Fluorescent “on–off–on” probe based on copper peptide backbone for specific detection of Cu (II) and hydrogen sulfide and its applications in cell imaging, real water samples and test strips. Microchem J 2022;182:107848. https://doi.org/10.1016/j.microc.2022.107848.

[4] Nagarajan R, Ryoo HI, Vanjare BD, Gyu Choi N, Hwan Lee K. Novel phenylalanine derivative-based turn-off fluorescent chemosensor for selective Cu^{2+} detection in physiological pH. J Photochem Photobiol Chem 2021;418:113435. https://doi.org/10.1016/j.jphotochem.2021.113435.

[5] He L, Li Q, Zhang Y, Huang K, Du B, Liang L. A naphthalimide functionalized fluoran with AIE effect for ratiometric sensing Hg^{2+} and cell imaging application. Spectrochim Acta Mol Biomol Spectrosc 2023;296:122672.

[6] Hu L, Xie K, Gao A, Hu Y, Hou A. Synthesis of novel triazine-quinoline-appended naphthalimide sensors for Hg(II) recognition and their structure-activity relationship. Dyes Pigments 2022;199:110048.

[7] Li Y, Ren Z, Ge Y, Di C, Zhou J, Wu J, Jia L. A novel peptide fluorescent probe based on different fluorescence responses for detection of Mercury species and hydrogen sulfide. Microchem J 2023;184:108160.

[8] Duarte F, Pereira-Gomes I, Dobrikov GM, Galhano J, Gomes CSB, Kurutos A, Santos HM, Oliveira E, Paula Duarte M, Luis Capelo-Martinez J, Lodeiro C. Antimicrobial profile and Turn-On sensing of cyanide and water traces using a dual chromophoric dansyl-acridine conjugate as multifunctional system. Microchem J 2024;205:111237.

[9] Xu H, Xiao Y, Liu Y, Sun W. Research progress on naphthalimide fluorescent probes. Adv Sensor Res 2024;3:2300032.

[10] Gao YG, Dang K, Zhang WJ, Liu FL, Patil S, Qadir A, Ding AX, Qian AR, A 1,8-naphthalimide-[12]. aneN_3 derivative for efficient Cu^{2+} recognition, lysosome staining and siRNA delivery. Colloids Surf B Biointerfaces 2022;185:110607.

[11] Bao Z, Qin C, jun Wang J, Sun J, Dai L, Chen G, Mei F. A sensitive and selective probe for visual detection of Cu^{2+} based on 1,8-naphthalimidederivative. Sens Actuators B Chem 2018;265:234–41.

[12] Wang H, Cui J, Fang X, Zhang W, Wang J, Chen S, Qian J. Fluorescent detection of copper ions with acylhydrazine-based probes: effects of substitute and its position. Dyes Pigments 2022;197:109954.

[13] Ho FC, Huang YJ, Weng CC, Wu CH, Li YK, Wu JI, Lin HC. Efficien t FRET approaches toward Copper(II) and cyanide detections via host−guest interactions

of photo-switchable [2]Pseudo-Rotaxane polymers containing naphthalimide and merocyanine moieties. ACS Appl Mater Interfaces 2020;12:53257–73.
[14] Liu C, Xu J, Yang F, Zhou W, Li Z, Wei L, Yu M. Nanomolar $Cu^{2+}$and F^{-} naked-eye detection with a 1,8-naphthalimide-based colorimetric probe. Sens Actuators B Chem 2015;212:364–70.
[15] Li Z, Hou JT, Wang S, Zhu L, He X, Shen J. Recent advances of luminescent sensors for iron and copper: platforms, mechanisms, and bio-applications. Coord Chem Rev 2022;469:214695.
[16] Ghosh S, Ghosh S, Ranjan Dhara S, Baildya N, Ghosh K. Naphthalimide-based new architecture for fluorescence turn-on sensing of Cu^{2+} and colorimetric detection of F^{-}/CN^{-}. Methods 2024;225:13–9.
[17] Cai H, Liang Y, Huang L, Wang J. Relay detection of Cu^{2+} and bovine serum albumin by a dansyl derivative-based fluorescent probe. Spectrochim Acta Mol Biomol Spectrosc 2022;277:121281.
[18] Guo Z, Wang Q, Zhou D, An Y, Wang P, Liao F. A novel peptide-based fluorescent probe with a large stokes shift for rapid and sequential detection of Cu^{2+} and CN^{-} in aqueous systems and live cells. Spectrochim Acta Mol Biomol Spectrosc 2022;264:120257.
[19] Liu YL, Yang L, Li P, Li SJ, Li L, Pang XX, Ye F, Fu Y. A novel colorimetric and "turn-off" fluorescent probe based on catalyzed hydrolysis reaction for detection of Cu^{2+} in real water and in living cells. Spectrochim Acta Mol Biomol Spectrosc 2020;227:117540.
[20] Fu Y, Pang XX, Wang ZQ, Chai Q, Ye F. A highly sensitive and selective fluorescent probe for determination of Cu(II) and application in live cell imaging. Spectrochim Acta Mol Biomol Spectrosc 2019;208:198–205.
[21] Guo B, Pan X, Liu Y, Nie L, Zhao H, Liu Y, Jing J, Zhang X. A reversible water-soluble naphthalimide-based chemosensor for imaging of cellular copper(II) ion and cysteine. Sens Actuators B Chem 2018;256:632–8.
[22] Liu Y, Jiang B, Zhao L, Zhao L, Wang Q, Wang C, Xu B. A dansyl-based fluorescent probe for sensing Cu^{2+} in aqueous solution. Spectrochim Acta Mol Biomol Spectrosc 2021;261:120009.
[23] Liang S, Tong Q, Qin X, Liao X, Li Q, Yan G. A hydrophilic naphthalimide-based fluorescence chemosensor for Cu^{2+} ion: sensing properties, cell imaging and molecular logic behavior. Spectrochim Acta Mol Biomol Spectrosc 2020;230:118029.
[24] Park SY, Kim W, Park SH, Han J, Lee J, Kang C, Lee MH. An endoplasmic reticulum-selective ratiometric fluorescent probe for imaging a copper pool. Chem Comm 2017;53:4457–60.
[25] Jiang H, Li Z, Kang Y, Ding L, Qiao S, Jia S, Luo W, Liu W. A two-photon fluorescent probe for Cu^{2+}based on dansyl moiety and its application in bioimaging. Sens Actuators B Chem 2017;242:112–7.
[26] Uttam B, Polepalli S, Sinha S, Majumder A, Rao CP. Selective sensing and removal of mercury ions by encapsulating dansyl appended Calix[4]Conjugate in a zeolitic imidazolate framework as an organic−inorganic hybrid nanomaterial. ACS Nano Mater 2022;5:11371–80.
[27] Cheng H, Yi F, Sun J, Li A, Zhang X, Guan D, Qu Y, Cao J. A naphthalimide-based fluorescent probe with a benzoylthiourea trigger for detection of Hg(II) in cosmetics. Dyes Pigments 2024;226:112135.
[28] Yang C, Li Y, Wu N, Zhang Y, Feng W, Yu M, Li Z. Ratiometric upconversion luminescence nanoprobes for quick sensing of Hg^{2+} and cells imaging. Sens Actuators B Chem 2021;326:128841.
[29] Pang X, Dong J, Gao L, Wang L, Yu S, Kong J, Li L. Dansyl-peptide dual-functional fluorescent chemosensor for Hg^{2+} and biothiols. Dyes Pigments 2020;173:107888.
[30] Aliberti A, Vaiano P, Caporale A, Consales M, Ruvo M, Cusano A. Fluorescent chemosensors for Hg^{2+} detection in aqueous environment. Sens Actuators B Chem 2017;247:727–35.
[31] Shinohara Y, Tsukamoto K, Maeda H. A fluorescent turn-on probe for Hg^{2+} with a high contrast designed by manipulating functional groups tethered to naphthalimide. J Photochem Photobiol Chem 2019;371:407–13.
[32] Wang P, An Y, Wu J. Highly sensitive turn-on detection of mercury(II) in aqueous solutions and live cells with a chemosensor based on tyrosine. Spectrochim Acta Mol Biomol Spectrosc 2020;230:118004.
[33] Graves M, Elioff MS, Knorr ES, Griffith JB, Hu J. A fluorescent turn-on sensor for Mercury (II) ions in near neutral poly (metharylic acid) solution. Spectrochim Acta Mol Biomol Spectrosc 2022;282:121702.
[34] Srivastava P, Verma M, Sivakumar S, Patra AK. A smart FRET probe exhibiting a molecular keypad lock device based on rapid detection of nitric oxide mediated by Cu^{2+} ion. Sens Actuators B Chem 2019;291:478–84.
[35] Mishra T, Guria S, Sadhukhan J, Das D, Das MK, Adhikari SS, Maity S, Maiti P. A naphthalimide appended rhodamine based biocompatible fluorescent probe: chemosensor for selective detection of Hg^{2+} ion, live cell imaging and DFT study. J Photochem Photobiol Chem 2024;446:115168.
[36] Gao J, He Y, Chen Y, Song D, Zhang Y, Qi F, Guo Z, He W. Reversible FRET fluorescent probe for ratiometric tracking of endogenous Fe^{3+} in ferroptosis. Inorg Chem 2020;59:10920–7.
[37] Lee HJ, Cho MJ, Chang SK. Ratiometric signaling of hypochlorite by the oxidative cleavage of Sulfonhydrazide-Based rhodamine−dansyl dyad. Inorg Chem 2015;54:8644–9.
[38] Martins F, Granja A, Reis S, Gameiro P, Barone G, Neves MGPMS, Silva AMG. Synthesis, fluorescence and theoretical insights into a novel FRET-Based dansyl-rhodamine sensor for the in vitro detection of toxic bioaccumulated Hg(II) ions. Spectrochim Acta Mol Biomol Spectrosc 2025;329:125534.
[39] Li N, Qin W, Chen Y, Liu K, Wang S, Kong F. Construction of a robust polarity sensitive platform and its application for tracking of lipid droplets decrease under oxidative stress in live cells. Sens Actuators B Chem 2021;346:130491.
[40] Yang D, Wu XT, Cao XJ, Zhao BX. A reversible ratiometric fluorescence probe for fast detection of trace water in different organic solvents. Dyes Pigments 2019;170:107558.
[41] Zheng C, Zhang X, Gao A, Ju M, Hou A, Xie K. Adjustable multimodality fluorescence emissions and photochromism of functional molecular device containing double chromophores with intramolecular FRET process. Dyes Pigments 2024;228:112238.
[42] Zhao J, Zhang J, Hu B, Gao C, Li Z, Sun Z, You J. Spectrochim Acta Mol Biomol Spectrosc 2023;286:121965.
[43] Lee H, Lee HS, Reibenspies JH, Hancock RD. Mechanism of "Turn-on" fluorescent sensors for Mercury(II) in solution and its implications for ligand design. Inorg Chem 2012;51:10904–15.
[44] Deng W, Li S, Zhou M, Zheng M, Wang P, An Y. Ratiometric peptide-based fluorescent probe with large stokes shift for detection of Hg^{2+} and S^{2-} and its applications in cells imaging and smartphone-assisted recognition. Spectrochim Acta Mol Biomol Spectrosc 2024;315:124306.
[45] Zhang L, Zhao P, Yu S, Kong J, Gao L, Li L. Dansyl-modified tryptophan fluorescence sensor for highly sensitive and selective detection of Hg^{2+} in aqueous solutions. Microchem J 2024;200:110520.
[46] Tamizhselvi R, Bhaskar R, Beena M, Palaniappan A, Kumar SKA, Napoleon AA. A dual responsive bis-thiophene affixed thiosemicarbazide based chemosensor for colorimetrically Hg^{2+} and fluorometrically Cu^{2+} ions and their applications in live cell imaging. Spectrochim Acta Mol Biomol Spectrosc 2024;322:124766.
[47] Shi WJ, Li CF, Huang Y, ya Tan H, Wei YF, Liu F, Feng LX, Zheng L, Chen GS, wu Yan J. A remarkable colorimetric probe for fluorescent ratiometric and ON-OFF discriminative detection of Hg^{2+} and Cu^{2+} by double-channel imaging in living cells. Dyes Pigments 2019;171:107782.
[48] Chang LL, Gao Q, Liu S, Hu CC, Zhou WJ, Zheng MM. Selective and differential detection of Hg^{2+} and Cu^{2+} with use of a single rhodamine hydrazone-type probe in the absence and presence of UV irradiation. Dyes Pigments 2018;153:117–24.
[49] [a] Kundu N, Maity M, Chatterjee PB, Teat SJ, Endo A, Chaudhury M. Reporting a Unique Example of Electronic Bistability Observed in the Form of Valence Tautomerism with a Copper(II) Helicate of a Redox-Active Nitrogenous Heterocyclic Ligand. J Am Chem Soc 2011;133:20104–7.[b] Sato O, Tao J, Zhang YZ. Control of Magnetic Properties through External Stimuli. Angew Chem Int Ed 2007;46:2152–87.
[50] Sato O, Tao J, Zhang YZ. Control of magnetic properties through external stimuli. Angew Chem Int Ed 2007;46:2152–87. https://doi.org/10.1002/anie.200602205.
[51] Wiesner S, Wagner A, Kaifer E, Himmel HJ. A valence tautomeric dinuclear copper tetrakisguanidine complex. Chem Eur J 2016;22:10438–45.
[52] Tezgerevska T, Alley KG, Boskovic C. Valence tautomerism in metal complexes: stimulated and reversible intramolecular electron transfer between metal centers and organic ligands. Coord Chem Rev 2014;268:23–40.
[53] Gransbury GK, Livesay BN, Janetzki JT, Hay MA, Gable RW, Shores MP, Starikova A, Boskovic C. Understanding the origin of one-ortwo-step valence tautomeric transitions in bis(dioxolene)-bridged dinuclear cobalt complexes. J Am Chem Soc 2020;142:10692–704.
[54] Hess KM, Leach IF, Wijtenhorst L, Lee H, Klein JEMN. Valence tautomerism induced proton coupled electron transfer: X-H bond oxidation with a dinuclear Au (II) hydroxide complex. Angew Chem Int Ed 2024;63:e202318916.
[55] Lonnon DG, Sang TL, Colbran SB. Valence tautomerism and coordinative lability in Copper(II)-Imidazolyl-Semiquinonate anion radical models for the Cu_B center in cytochrome *c* oxidases. J Am Chem Soc 2007;129:5800–1.
[56] Sambiagio C, Marsden SP, Blacker AJ, McGowan PC. Copper catalysed ullmann type chemistry: from mechanistic aspects to modern development. Chem Soc Rev 2014;43:3525–50.
[57] Andrada DM, Soria-Castro SM, Caminos DA, Argüello JE, Peñéñory AB. Understanding the heteroatom effect on the ullmann copper-catalyzed cross-coupling of X-Arylation (*X* =NH, O, S) mechanism. Catalysts 2017;7:388.
[58] Strekalova S, Kononov A, Rizvanov I, Budnikova Y. Acetonitrile and benzonitrile as versatile amino sources in copper-catalyzed mild electrochemical C–H amidation reactions. RSC Adv 2021;11:37540–3.
[59] Xu Z, Zhang MX, Li G, Chen X, Liu SH, Chen H, Yin J. Naphthalimide-sulfonamide fused dansyl-sulfonamide fluorescent probe for tracking glutathione of lysosome with a dual-emission manner. Dyes Pigments 2019;171:107685.
[60] Das S, Sahoo P. A colorimetric sensor for hydrogen sulfide: detection from biogas and quantitative estimation in water. Sens Actuators B Chem 2019;291:287–92.
[61] Bin Li K, Zhou D, He XP, Chen GR. Ratiometric glyco-probe for transient determination of thiophenol in full aqueous solution and river water. Dyes Pigments 2015;116:52–7.
[62] Kong Y, Wan X, Liu Z, Chen F, Wu F, Qin G, Cao D, Cui Y. A novel dansyl-naphthalimide fluorescent probe for visualizing nitroxyl (HNO) in biological systems. Sens Actuators B Chem 2022;350:130852.
[63] Bagherzadeh N, Reza Sardarian A. Green approach to new library of 1,8-naphthalimide fluorophores employing C-C and C-N cross coupling reactions by novel, durable, and reusable magnetic nanocatalyst bearing nickel (0) complex of 1,10-phenanthroline. J Photochem Photobiol Chem 2024;449:115345.
[64] Huang G, Li C, Han X, Aderinto SO, Shen K, Mao S, Wu H. Sensitive and selective detection of Cu(II) ion: a new effective 1,8-naphthalimide-based fluorescence 'turn off' sensor. Luminescence 2018;33:660–9.
[65] Schulz A, Wotschadlo J, Heinze T, Mohr GJ. Fluorescent nanoparticles for ratiometric pH-monitoring in the neutral range. J Mater Chem 2010;20:1475–82.
[66] Benanti TL, Saejueng P, Venkataraman D. Segregated assemblies in bridged electron-rich and electron-poor p-conjugated moieties. Chem Comm 2007:692–4.

[67] Chinapang P, Ruangpornvisuti V, Sukwattanasinitt M, Rashatasakhon P. Ferrocenyl derivative of 1,8-naphthalimide as a new turn-on f luorescent sensor for Au(III) ion. Dyes Pigments 2015;112:236–8.
[68] Pfeffer FM, Seter M, Lewcenko N, Barnett NW. Fluorescent anion sensors based on 4-amino-1,8-naphthalimide that employ the 4-amino N–H. Tetrahedron Lett 2006; 47:5241–5.
[69] Lim T, Ryoo JY, Jang M, Han MS. Ligand-free suzuki–miyaura cross-coupling with low Pd content: rapid development by a fluorescence-based high-throughput screening method. Org Biomol Chem 2021;19:1009–16.
[70] Ohtani R, Anegawa Y, Watanabe H, Tajima Y, Kinoshita M, Matsumori N, Kawano K, Yanaka S, Kato K, Nakamura M, Ohba M, Hayami S. Metal complex lipids for fluid–fluid phase separation in coassembled phospholipid membranes. Angew Chem Int Ed 2021;60:13603–8.
[71] Cheng K, Zheng QZ, Qian Y, Shi L, Zhao J, Zhu HL. Synthesis, antibacterial activities and molecular docking studies of peptide and schiff bases as targeted antibiotics. Bioorg Med Chem 2009;17:7861–71.
[72] Dash SC, Dash AC. Proximity effect on the general base catalysed hydrolysis of amide linkage: the role of cationic surfactant, CTABr. J Chem Sci 2011;123: 497–507.
[73] Oliveira E, Baptista RMF, Costa SPG, Raposo MMM, Lodeiro C. Solvatochromic effects of bis(indolyl)thienylaril derivatives as new colored materials. Photochem Photobiol Sci 2014;13:492–8.
[74] Mocanu S, Ionita G, Matei I. Solvatochromic characteristics of dansyl molecular probes bearing alkyl diamine chains. Spectrochim Acta Part A Mol Biomol Spectrosc 2020;237:118413.
[75] Nolan EM, Lippard SJ. Tools and tactics for the optical detection of mercuric ion. Chem Rev 2008;108:3443–80.
[76] Gans P, Sabatini A, Vacca A. Investigation of equilibria in solution. Determination of equilibrium constants with the HYPERQUAD suite of programs. Talanta 1996; 43:1739–53.
[77] Peisach J, Blumberg WE. Structural implications derived from the analysis of electron paramagnetic resonance spectra of natural and artificial copper proteins. Arch Biochem Biophys 1974;165:691–708.
[78] Biesinger MC. Advanced analysis of copper X-ray photoelectron spectra. Surf Interface Anal 2017;49:1325–34.
[79] Alders D, Voogt FC, Hibma T, Sawatzky GA. Nonlocal screening effects in 2 p x-ray photoemission spectroscopy of NiO (100). Phys Rev B 1996;54:7716–9.